Comparison of Analysis, Simulation, and Measurement of Wire-to-Wire Crosstalk, Part 2

Arthur T. Bradley[#1], Brian J. Yavoich[#2], Shane M. Hodson[#3], Richard F. Godley[#4]

NASA Langley Research Center

5 North Dryden, MS488, Hampton, VA 23681 USA

[1]arthur.t.bradley@nasa.gov

[2]brian.yavoich@fandm.edu

[3]smh7zy@virginia.edu

[4]rgodley@gmail.com

***Abstract*— In this investigation, we compare crosstalk analysis, simulation, and measurement results for electrically short configurations. Methods include hand calculations, PSPICE simulations, Microstripes transient field solver, and empirical measurement. In total, four representative physical configurations are examined, including a single wire over a ground plane, a twisted pair over a ground plane, generator plus receptor wires inside a cylindrical conduit, and a single receptor wire inside a cylindrical conduit. Part 1 addresses the first two cases, and Part 2 addresses the final two. Agreement between the analysis methods and test data is shown to be very good.**

I. Introduction

This paper represents the second part of a two-paper investigation into comparing crosstalk analyses, simulations, and experimental results. In the first paper, single wire and twisted pair wiring were examined. In this second paper, we examine two additional cases. The first is a noisy generator wire and passive receptor wire both enclosed in a solid conducting conduit. The second case has the receptor wire inside the shielding conduit, with the generator wire outside.

With each configuration, the system was first modeled using per-unit-length capacitances and inductances (both self and mutual). This served as a distributed lumped model representation of the electromagnetic coupling and offered a straightforward method with which to perform hand calculations and PSPICE simulations. In all cases, per unit impedances were determined using the equations given in [1].

Simulations were completed using both PSPICE and CST's Microstripes – a time-domain field solver that uses the transmission line matrix (TLM) method. That method "meshes" the physical model in three dimensions and treats each piece as a transmission line structure.

Measurements of V_{NE} and V_{FE} were taken across the near- and far-end resistors, R_{NE} and R_{FE}, respectively. Resistors R_{NE} and R_{FE} were varied from 20Ω - 1960Ω, but kept equal to each other. Resistor R_L was also independently varied. V_S was adjusted for every test case to apply a constant 1.75V amplitude 5MHz sinusoid across the load resistor, allowing the losses associated with R_S to be removed from the analysis.

The importance of this work is twofold. First, it clearly demonstrates the applicability (and limitations) of lumped circuit crosstalk analyses. It also identifies and discusses important crosstalk effects only discernible from varying system impedances. Such discussion is not typically included in prevalent literature which focuses instead on studying crosstalk across varying frequencies.

II. Shielded Generator and Receptor Configuration

A. Hand Calculations

For the third test case, the generator and receptor wires were routed parallel inside a cylindrical aluminum conduit shield. The setup is shown in Fig. 1.

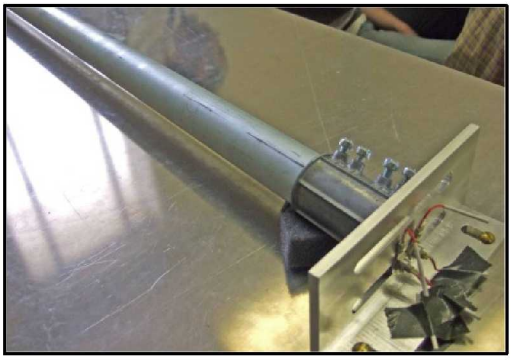

Fig. 1 Shielded generator and receptor configuration

The per-unit-length inductance and capacitance, and V_{NE}, V_{FE} equations were calculated with the following equations from [1].

$$l_G = \frac{\mu_o}{2\pi} \cdot \ln\left[\frac{r_{sh}^2 - d_G^2}{r_{sh} r_{wG}}\right] \quad (1)$$

$$l_R = \frac{\mu_o}{2\pi} \cdot \ln\left[\frac{r_{sh}^2 - d_R^2}{r_{sh} r_{wR}}\right] \quad (2)$$

$$l_m = \frac{\mu_o}{2\pi} \cdot \ln\left[\frac{d_R}{r_{SH}} \sqrt{\frac{(d_G d_R)^2 + r_{SH}^2 - 2 d_G d_R r_{SH}^2 \cos(\theta_{GR})}{(d_G d_R)^2 + d_R^4 - 2 d_G d_R^3 \cos(\theta_{GR})}}\right] \quad (3)$$

$$c_m = \frac{l_m}{v^2 (l_G l_R - l_m^2)} \quad (4)$$

$$c_G = \frac{l_R}{v^2 (l_G l_R - l_m^2)} - c_m \quad (5)$$

$$c_R = \frac{l_G}{v^2 (l_G l_R - l_m^2)} - c_m \quad (6)$$

Where r_{sh} is the inner radius of the pipe, d is the radial distance of the wire measured from the center of the conduit, and θ_{GR} is the separation angle of the wires. Once again, the standard wire-to-wire crosstalk equations were used to predict V_{NE} and V_{FE}.

$$V_{NE} = \left[\frac{R_{NE}}{R_{NE}+R_{FE}} j\omega L_m \frac{1}{R_S+R_L} V_S\right] + \left[\frac{R_{NE}R_{FE}}{R_{NE}+R_{FE}} j\omega C_m \frac{R_L}{R_S+R_L} V_S\right] \quad (7)$$

$$V_{FE} = \left[\frac{-R_{FE}}{R_{NE}+R_{FE}} j\omega L_m \frac{1}{R_S+R_L} V_S\right] + \left[\frac{R_{NE}R_{FE}}{R_{NE}+R_{FE}} j\omega C_m \frac{R_L}{R_S+R_L} V_S\right] \quad (8)$$

B. Simulations

Simulations were completed using both PSPICE and CST's Microstripes – a time-domain field solver that uses the transmission line matrix (TLM) method. That method "meshes" the physical model in three dimensions and treats each piece as a transmission line structure.

The per-unit-length circuit model parameters calculated for hand calculations were also fed directly into PSPICE. The PSPICE circuit is identical for the unshielded single-wire case (but with different per-unit-length impedances), given as Fig. 2. The inductive coupling between generator and receptor circuits was achieved using the PSPICE K-Coupling element. Capacitive coupling was achieved through the inclusion of C_M.

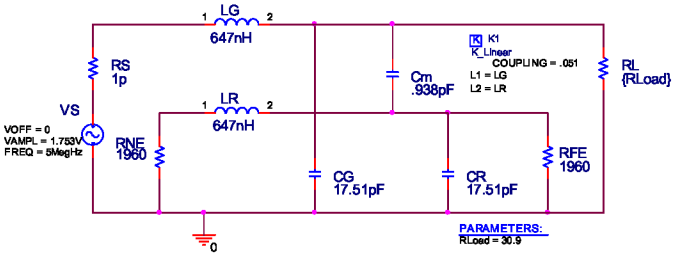

Fig. 2 PSPICE shielded generator and receptor model

Microstripes model creator was used to generate a 3D representation of the crosstalk assembly. The software tool allows either the importing of CAD files or the direct drawing of physical systems. Geometries as well as the electromagnetic properties of all materials are considered during simulation.

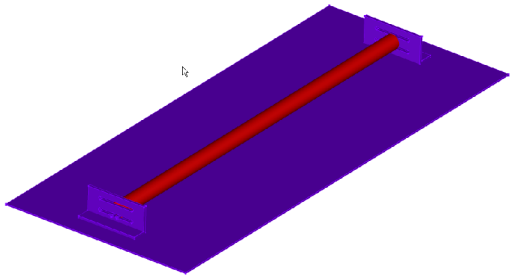

Fig. 3 Microstripes model

C. Results

For the shielded generator + receptor wire case, the results obtained from all four methods (experimentation, hand calculations, PSPICE, and Microstripes) were in reasonable agreement, with some minor discrepancies seen using the field solver. The differences are attributed to difficulty in measuring the precise wire-to-conduit geometry.

Fig. 5 and Fig. 6 show the magnitude of V_{NE} and V_{FE} for the case when R_L was varied, with R_{NE} and R_{FE} held constant at 511Ω. As was with the unshielded case (see Part 1 of this paper series), three distinct regions of crosstalk coupling can be identified. In the first region, R_L is small, and the inductive coupling acts as the primary crosstalk mechanism. The inverse relation between generator current and load resistance causes both the near- and far-end crosstalk voltages to decrease with increasing R_L. As R_L further increases in value, a point is reached where V_{FE} essentially goes to zero as inductive and capacitive coupling cancel. The near-end voltage on the other hand is simply the sum of the capacitive and inductive terms. Finally, in the final region, R_L becomes large enough that the capacitive term becomes the dominant coupling mechanism. This causes V_{NE} and V_{FE} to approach a constant value as can easily be seen from (7) and (8).

Fig. 7 and Fig. 8 show the results obtained when R_{NE} and R_{FE} were varied for a constant R_L, again arbitrarily chosen to be 511Ω. For simplicity, R_{NE} and R_{FE} were kept equal as they were increased. The four methods once again generally agreed well (both in trend and values). Inductive coupling is the dominant mechanism for low values of R_L or R_{NE} and R_{FE}. For higher impedance values, capacitive coupling dominates. When increasing R_{NE} and R_{FE}, the near-end crosstalk voltages increase as expected from (7). Far-end crosstalk initially decreases due to the cancelation between inductive and capacitive terms. Beyond that point, the slope turns positive as capacitive coupling dominates. This also agrees with (8).

This configuration exhibited the same general trends of the single-wire case, but with significantly reduced coupling levels (both capacitive and inductive). The overall conduit shield reduces the net coupling between the generator and receptor wire by essentially acting to create wire images with greater separation distances, as shown in Fig. 4. This effect is discussed in [1].

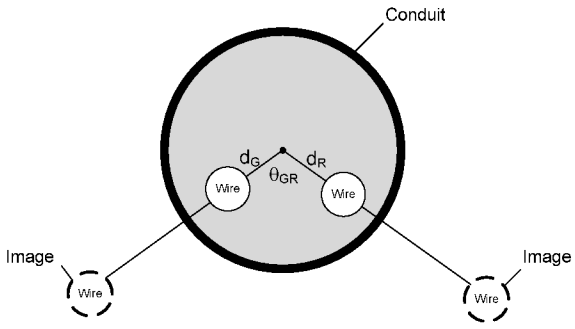

Fig. 4 Conduit diagram

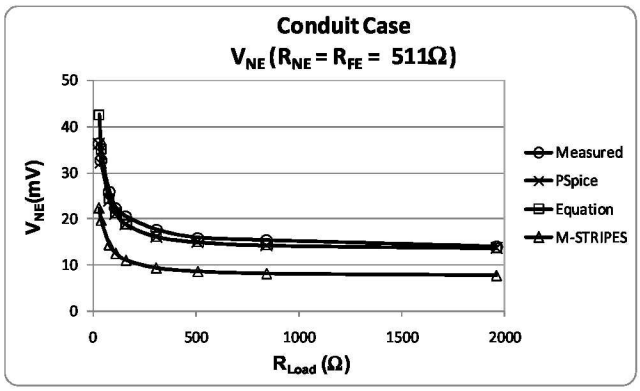

Fig. 5 V_{NE}, vary R_L, Conduit

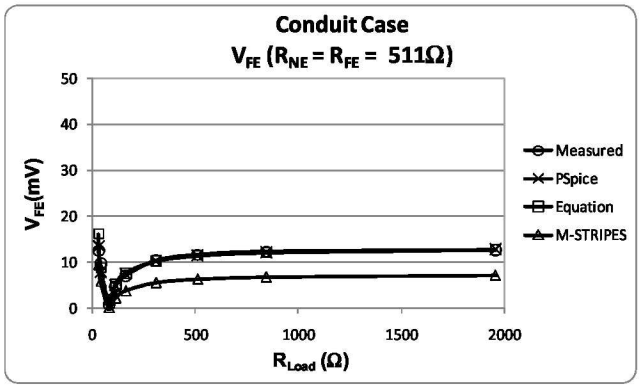

Fig. 6 V_{FE}, vary R_L, Conduit

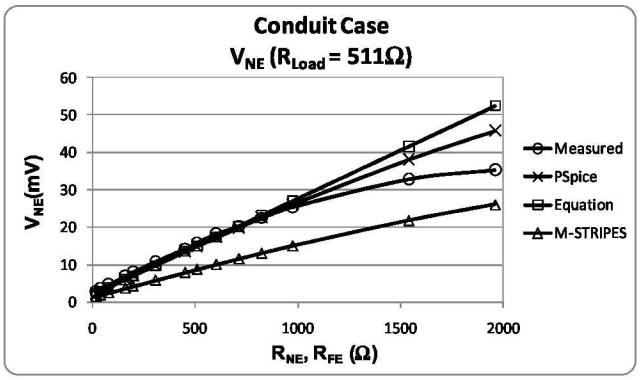

Fig. 7 V_{NE}, vary R_{NE} R_{FE}, Conduit

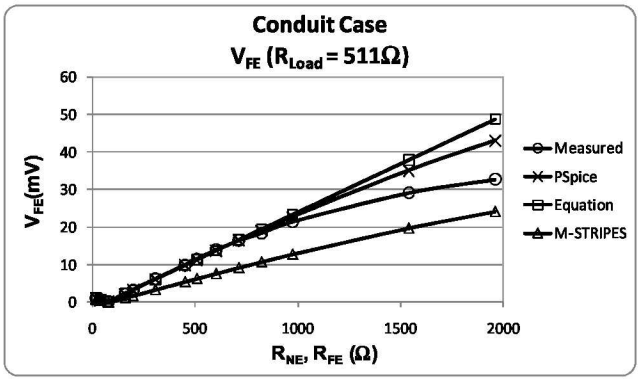

Fig. 8 V_{FE}, vary R_{NE} R_{FE}, Conduit

III. Shielded Receptor (One or Both Ends Grounded)

The fourth case involved running a single receptor wire inside a cylindrical aluminum conduit shield. A single generator wire ran parallel to the shield. The shield termination was varied from being grounded either at the near end only or both the near and far ends. The setup is shown in Fig. 9.

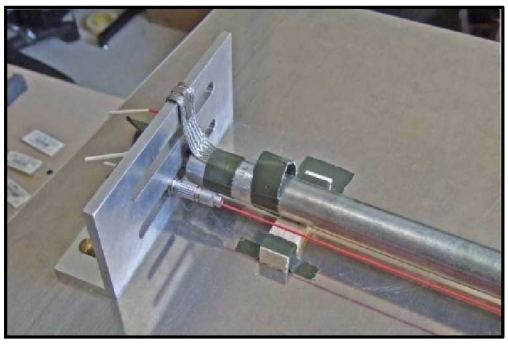

Fig. 9 Shielded receptor configuration

The per-unit-length inductances and capacitances were calculated with equations given in [1] – not repeated here for brevity. Those feed directly into the near- and far-end voltage calculations, V_{NE} and V_{FE} as shown below.

Shield grounded at near end:

$$V_{NE} = j\omega\left[\frac{R_{NE}}{R_{NE}+R_{FE}}\frac{L_{GR}}{R_S+R_L}\right]V_S \quad (9)$$

$$V_{FE} = j\omega\left[\frac{-R_{FE}}{R_{NE}+R_{FE}}\frac{L_{GR}}{R_S+R_L}\right]V_S \quad (10)$$

Shield grounded at both ends:

$$V_{NE} = \left[\frac{R_{NE}}{R_{NE}+R_{FE}}\frac{L_{GR}}{R_S+R_L}\right]\cdot\left[\frac{R_{SH}}{L_{SH}}\right]V_S \quad (11)$$

$$V_{FE} = j\omega\left[\frac{-R_{FE}}{R_{NE}+R_{FE}}\frac{L_{GR}}{R_S+R_L}\right]\cdot\left[\frac{R_{SH}}{L_{SH}}\right]V_S \quad (12)$$

From basic field theory, one would expect a reduction in crosstalk due to the shielding. For the single-ended shield connection, shown in Fig. 10 - Fig. 13, inductive coupling is still present at low values of R_L. But as R_L increases, the coupling drops off rapidly towards the near zero level of capacitive coupling. For the shield connected at both ends, both the inductive and capacitive coupling are greatly reduced as shown in Fig. 14 - Fig. 17. The coupled voltages remain essentially flat due to the constant ratio [R_{NE} / (R_{NE} + R_{FE})]. Inductive coupling reduction is due to the magnetic flux cancelation between the generator currents and shield currents. Experimental data was slightly higher than predicted levels due to measurement limitations and ambient noise levels.

IV. References

[1] C.R. Paul, *Introduction to Electromagnetic Compatibility*, 2nd ed., Wiley Interscience, New Jersey, 2006.

[2] H.W. Ott, *Noise Reduction Techniques in Electronic Systems*, 2nd ed., Wiley Interscience, New York, 1988.

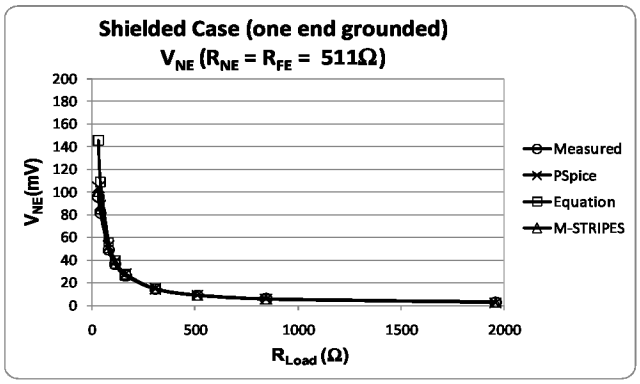

Fig. 10 V_{NE}, vary R_L, Shielded (one end grounded)

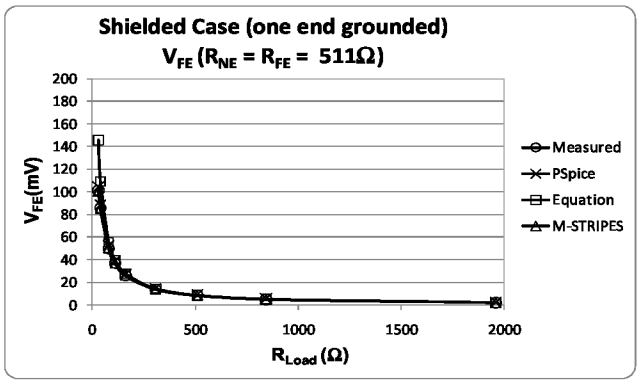

Fig. 11 V_{FE}, vary R_L, Shielded (one end grounded)

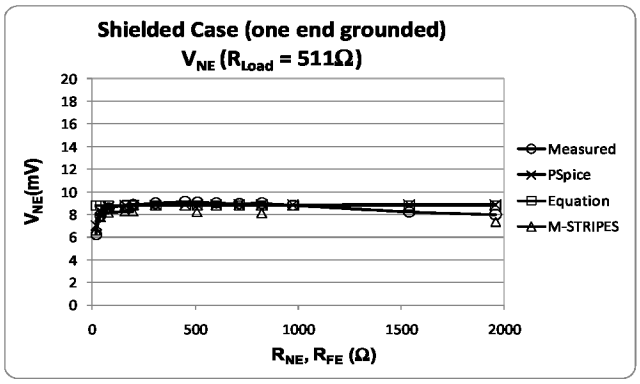

Fig. 12 V_{NE}, vary R_{NE} R_{FE}, Shielded (one end grounded)

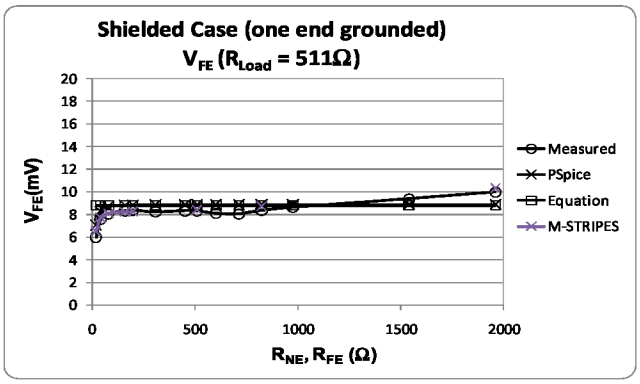

Fig. 13 V_{FE}, vary R_{NE} R_{FE}, Shielded (one end grounded)

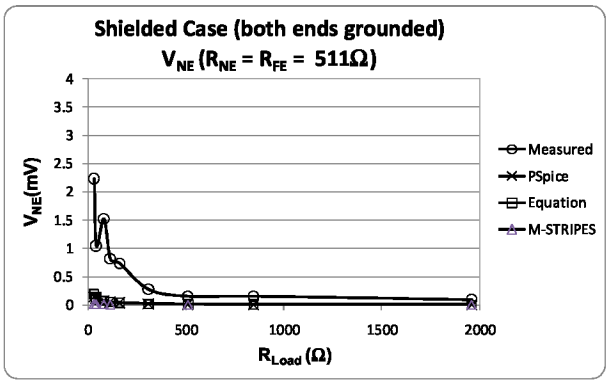

Fig. 14 V_{NE}, vary R_L, Shielded (both ends grounded)

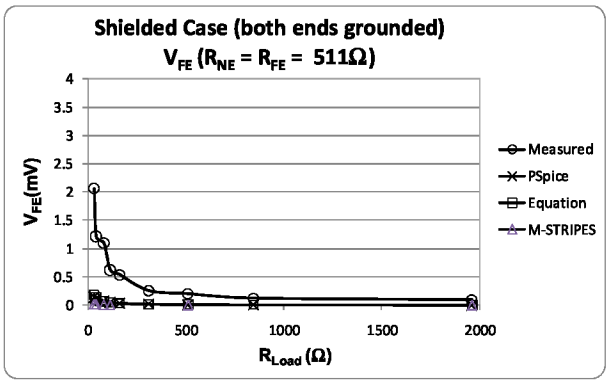

Fig. 15 V_{FE}, vary R_L, Shielded (both ends grounded)

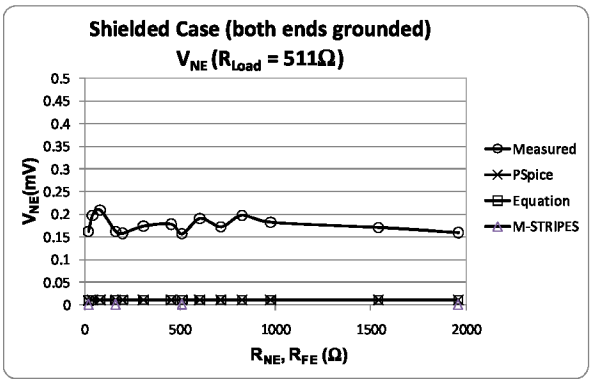

Fig. 16 VNE, vary RNE RFE, Shielded (both ends grounded)

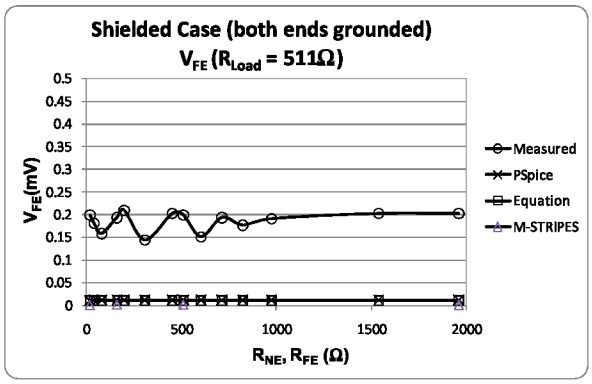

Fig. 17 VFE, vary RNE RFE, Shielded (both ends grounded)